Available online at www.sciencedirect.com
ScienceDirect
Journal of Solid State Chemistry 179 (2006) 2761–2767
JOURNAL OF SOLID STATE CHEMISTRY
www.elsevier.com/locate/jssc

Peculiarities in the Raman spectra of ZrB_{12} and LuB_{12} single crystals

H. Werheit[a,*], Yu. Paderno[b], V. Filippov[b], V. Paderno[b], A. Pietraszko[c], M. Armbrüster[d], U. Schwarz[d]

[a]*Institute of Physics, University Duisburg-Essen, Campus Duisburg, 47048 Duisburg, Bensberger Marktweg 328, D-51069 Köln, Germany*
[b]*I.N.Frantsevich Institute for Problems of Materials Science of NASU, 3 Krzhyzhanovsky Street, 03142 Kiev, Ukraine*
[c]*Institute of Low Temperatures and Structure Research, Wroclaw, Poland*
[d]*Max-Plank-Institut für Chemische Physik fester Stoffe, Nöthnitzer Street 40, 01187 Dresden, Germany*

Received 7 September 2005; received in revised form 21 November 2005; accepted 29 November 2005
Available online 9 January 2006

Abstract

We have measured Raman spectra of high-quality $Zr^{nat}B_{12}$, $Lu^{nat}B_{12}$ and $Lu^{11}B_{12}$ single crystals with high resolution, and the observed strong peaks are attributed to specific vibration modes. Besides, there are a number of additional Raman peaks in spectral ranges, where only Raman-inactive vibrations of the atomic arrangement are expected. Accordingly, it is assumed, that the investigated crystals contain intrinsic structural imperfections or distortions in sufficient concentration and efficiency to initiate the observed breaking of phonon selection rules. We suppose boron vacancies, boron isotope effects and displacements of the metal atoms to be reasons for such imperfections.

Keywords: ZrB_{12}; $Lu^{nat}B_{12}$; $Lu^{11}B_{12}$; Raman spectra; Structural imperfections; Vacancies; Isotope effects; Metal atom displacements

1. Introduction

Metal–boron refractory compounds are widely used in modern techniques due to their unique combination of properties (see [1,2]), such as high melting points, hardness, thermal as well as chemical stability. Moreover, these compounds are model substances for numerous physical investigations, for example to determine the different boron sub-lattices in MB_2, MB_4, MB_6, MB_{12} and MB_{66} phases (M = metal) with respect to the influence of the nature of the various metals or metal ions on the properties of the boride framework.

In this context the consideration of structural imperfections is very important. In solids with periodic structures defects are usually taken as weak deviations from the ideal atomic arrangement. However, for some complex boron structures (β-rhombohedral boron and boron carbide) it was proven that disregarding structural defects in band structure calculations leads to fundamental errors in the determination of electronic properties. In extreme cases, e.g. that of boron carbide, metallic character instead of semiconducting behavior was predicted (see [3,4]). At present, it remains to be investigated if in binary boron compounds like metal hexaborides and dodecaborides the influences of structural imperfections, defects or distortions has similarly dramatic effects on the electronic properties.

The investigated boron compounds MB_{12} (M = Lu, Zr) may be considered as clathrate-like systems [5] comprising two sub-structures—the very rigid boron cages and the relatively weakly bonded metal atoms with atomic diameters, which are often distinctly smaller than the accommodating voids of the anionic boron framework. Nevertheless, while the rigid boron network essentially determines mechanical and related properties, the metal atoms and their oxidation states preferably determine electronic transport and magnetic properties. For instance, the electrical conductivity of MB_6 phases can vary from insulating (CaB_6) to metallic behavior (LaB_6 and some others). Hardness and chemical resistance of the boride

*Corresponding author. Fax: +49 221 682796.
E-mail address: helmut.werheit@koeln.de (H. Werheit).

0022-4596/$ - see front matter © 2005 Elsevier Inc. All rights reserved.
doi:10.1016/j.jssc.2005.11.034

phases usually increase with the boron content increasing. After the recent discovery of high-T superconductivity in the otherwise well-known MgB_2 [6], all boride phases newly attracted the attention of physicists, inorganic chemists and material scientists.

The same holds for rare-earth metal dodecaborides REB_{12}, (RE = rare-earth metal), for which overviews on properties have been accomplished [7–10]. Zirconium dodecaboride ZrB_{12} is a member of this structure family and it was synthesized as early as 1952; however, apart from the crystal structure, the knowledge of properties has remained very limited [11–15], although the Debye temperature was determined to correspond to 1040 K [16]. Band structure calculations were performed by Shein and Ivanovski [17], and metallic conductivity and superconductivity (T_c approximately 6 K) are known [18]. Crystal structure and composition imply a similarity to YB_{12}, UB_{12}, REB_{12}, (RE = rare-earth metal) which are characterized by unusual physical properties like mixed valency, heavy fermion behavior, superconductivity, and specific magnetic transitions.

For the stability range of ZrB_{12} controversial data are given in the literature: A very large temperature range extending from ambient conditions to the melting point has been reported, but also a very narrow one [19,20]. According to Massalski's constitutional diagram of the Zr–B binary system it is even limited to temperatures between 1696 and 2082 °C only, and the phase has a peritectic melting character [21]. Meanwhile, the preparation of ZrB_{12} single crystals, which are stable at ambient conditions [16,22], solved this controversy.

We report on Raman spectra of ZrB_{12} single crystals for the first time and compare these to measurements on LuB_{12}. According to the electron configuration $4d^2\ 5s^2$ for Zr and $5d^1\ 6s^2$ for Lu, different electron transfers to the boron substructures may be realized. The effect of these differences on Raman spectra will be taken into account.

2. Sample material

Large ZrB_{12} single crystals with a diameter of 6 mm and a length up to 40 mm [16] are prepared using pure natural boron (isotope distribution, 18.83% ^{10}B, 81.17% ^{11}B). X-ray diffraction diagrams of the crushed rod revealed only the presence of ZrB_{12}. Moreover, diagrams obtained from both ends of the large rod evidence single-crystalline character, and the cell parameter $a = 740.72(5)$pm agrees well within the estimated experimental error with the value of 740.75(1) pm, which was recently reported using much smaller single crystals obtained by an independent group [22], and is in agreement with an absence of soluble impurities in the studied crystals. The hydrostatically measured specific density of our single crystal corresponds to 3.60(2) g/cm^3 and is in good agreement with the density of 3.61 g/cm^3, which is calculated using the experimental lattice parameters and assuming full occupancy of all atomic sites. Hence, for ZrB_{12} a significant concentration of vacancies in the metallic sublattice (>1 at%) is highly improbable. A significantly higher concentration of vacancies in the boron framework cannot be ruled out due to the large atomic weight ratio Zr:B of approximately 9:1.

Preparation and some physical properties of the investigated LuB_{12} single crystals have been reported earlier [23]. The purity of the ingredient amorphous boron was 99.5% and that of the Lu_2O_3 99.9985%. The impurities are assumed to be nearly entirely removed during the boron reduction of the rare-earth metal oxide and the subsequent zone melting of the binary compound as evidenced by chemical analysis of the samples (oxygen below the detection limit of 0.25 wt%).

The total impurity content of the zone melted single crystals is below 10^{-3}%. A hydrostatic density determination yields results compatible with a composition $LuB_{11.83(6)}$ in close agreement to the chemical analysis leading to $LuB_{11.86(24)}$. These findings are consistent with a deficiency of boron atoms in the crystal structure [24].

The cell parameters of different crystals agree within a small uncertainty range (746.44(2) pm) indicating that this is the stable composition of the compound, and imperfections of the idealized structure like vacancies or distortions may be intrinsic. Intrinsic structural imperfections in the form of vacancies or anti-side defects occur in the structure of β-rhombohedral boron and boron carbide, both essentially based on B_{12} icosahedra as structural elements. There, these imperfections generate split-off valence states in the band gap, which drastically influence the electronic properties of these crystals [3,4].

3. Experimental

In order to gain plain sample surfaces, different preparation methods like cutting, lapping, polishing and etching were tested. The results of Raman investigations of differently treated specimen evidence that freshly broken samples manufactured from plates, which are cut from single crystals yield exactly reproducible Raman spectra and reliable spectral positions of the Raman lines. Accordingly, this preparation method was finally used for all investigated samples.

The Raman measurements were performed at ambient conditions with a Jobin Yvon Labram spectrometer using a HeNe laser of 15 mW for excitation and an 1800 g/mm grating. The spectral resolution corresponds to about 1 cm^{-1}. The laser spot size on the samples amounts to about 10 μm in diameter, and the employed notch filter of the equipment excluded Raman shifts below 100 cm^{-1} from detection. The spectra displayed below have been reproduced several times and on different samples each. Artifacts from the equipment have been excluded by crosschecking the spectra of several hexaborides. Therefore, even the weak Raman peaks are reliable. However, it cannot be definitely excluded that in the frequency range below about 200 cm^{-1} the shape of the Raman spectra is somewhat affected by the influence of the notch filter.

4. Results and discussion

The crystal structure of the investigated specimens (UB_{12} type) can be described in terms of a modified *fcc* unit cell with the metal atoms in the center of regular B_{24} truncated octahedra, with B atoms at each of their 24 vertices. An alternative description is a modified NaCl-type structure formed by metal atoms and B_{12} cubo-octahedra (see [10] and references therein). The atomic pattern bears a certain similarity to clathrate-type arrangements and may, thus, be considered to consist of two substructures, condensed boron clusters forming a 3D network and *RE* atoms, respectively. Since the links within the B_{12} cubo-octahedra are strong covalent bonds, the high melting points and the rigidity of the crystal structures can be attributed to the chemical bonding in the boron network.

When local distortions due to defect formation are not taken into account, the average structure adopts space group $Fm\bar{3}m$. For this idealized atomic pattern, the number of Raman active phonon modes Γ was estimated by a factor group analysis [25] to correspond to

$$\Gamma = A_{1g} + 2E_g + 2F_{2g}.$$

A_{1g}, E_g and F_{2g} are irreducible representations for O_h symmetry. These five phonons represent vibrations of the boron sublattice only. The vibrations of the metal ions are forbidden for Raman scattering because they are positioned on inversion centers. However, it must be obeyed that these considerations correspond to the idealized structure of the dodecaborides. Structural imperfections can more or less lift these selection rules, and in such cases additional modes appear in the Raman spectra.

In Fig. 1 the Raman spectra of $Zr^{nat}B_{12}$, $Lu^{nat}B_{12}$ and $Lu^{11}B_{12}$ are displayed. To obtain the fine structure of the Raman spectra with high accuracy, additional spectra of the same samples were obtained with five-fold integration time (typically 1500 s) to improve the signal-to-noise ratio (Fig. 2). The frequencies of the peak maxima are listed in Table 1. Because of the natural isotope distribution in the samples (18.83% ^{10}B and 81.17% ^{11}B), the Raman lines are significantly broadened towards higher frequencies. For a single vibrating boron atom the frequency shift due to the mass difference can be estimated to the factor,

$$\omega_1/\omega_2 = (m_2/m_1)^{1/2} = (m(B_{11})/m(B_{10}))^{1/2} = 1.0488.$$

Comparing the spectra of $Lu^{nat}B_{12}$ and $Lu^{11}B_{12}$ with the average boron atomic mass relation 11/10.8 the corresponding factor is 1.0092. The factors obtained from the strongest lines of the spectra of $Lu^{nat}B_{12}$ and $Lu^{11}B_{12}$ are listed in Table 2. The 784/774 cm^{-1} phonon exactly meets the expected value; for the others the quotient is somewhat larger, indicating that other bonding conditions like distances and bonding forces are not independent of the boron isotope and may influence the vibration frequencies as well. A deviation from the statistical distribution of the boron isotopes assumed for other structure groups of complex boron compounds could be a further reason for the frequency shift of lattice vibrations.

The polarization-dependent low-temperature Raman spectra reported by Fujita et al. [25] allow for attributing the measured Raman lines in Table 1 to four of the five specific vibration modes. The observed differences of line positions compared with the oriented and polarized low-temperature measurements [25] is in the range, which we found to be covered by different surface treatments. The phonon density distributions obtained using inelastic neutron scattering by Bouvet et al. [26] and Nefeodova et al. [27] allow assigning numerous of the weak structures in the Raman spectra to specific vibrations, which are not Raman active in the ideal lattice. However, based on more recent investigations on YbB_{12} Nemkovski et al. [28] question the interpretation by Bouvet et al. In particular this holds for the low-frequency range. The observation of these modes clearly evidences that the local structure of the boron cages has a lower symmetry than the average atomic pattern as determined by room temperature X-ray diffraction. In accordance with this result, more recent single-crystal diffraction experiments [29] indicate that at room temperature 1.33% of the lutetium atoms are located at positions slightly outside the cage centers.

Since the atomic pattern of ZrB_{12} is essentially the same as that of LuB_{12}, the vibration frequencies are expected to be only slightly shifted. Thus, the conclusions basically hold for ZrB_{12} as well. However, additional features are clearly seen in this spectrum. Obviously, the 1015 cm^{-1} phonon (E_g) and the 1043 cm^{-1} phonon (A_{1g}), which are nearly degenerate in LuB_{12}, are distinctly separated in ZrB_{12} (1012 and 1090 cm^{-1}). Moreover, in the range between these phonons two additional shoulders of Raman peaks are clearly detectable. The offset of metal atoms changes the boron–metal interaction, and, thus, the vibration frequency. This seems to be a possible explanation for such additional peaks. However, on the basis of present data, an unambiguous attribution is not yet possible.

At wavenumbers up to about 270 cm^{-1} several of the small peaks are found in the spectra of both compounds; however, for ZrB_{12} they superimpose a broad strong peak (218(2) cm^{-1}), which is absent in the LuB_{12} spectrum. If we hypothetically attribute this peak to a vibration of the Zr atom, the according vibration of Lu is expected at 158 cm^{-1} based on the mass-dependent frequency shift $\omega_{Lu}/\omega_{Zr} = (m_{Zr}/m_{Lu})^{1/2} = 1.38$, when equal bonding forces are assumed. Since it is reasonable to assume that the force constant is larger for the zirconium compound due to the higher charge of the metal atom as well as due to the reduced lattice parameter and, thus, shorter metal boron distances, the corresponding Raman peak of LuB_{12} is expected to be located at lower wave numbers and, thus, may be masked by the strongly decreasing background signal below approximately 200 cm^{-1} caused by the notch filter.

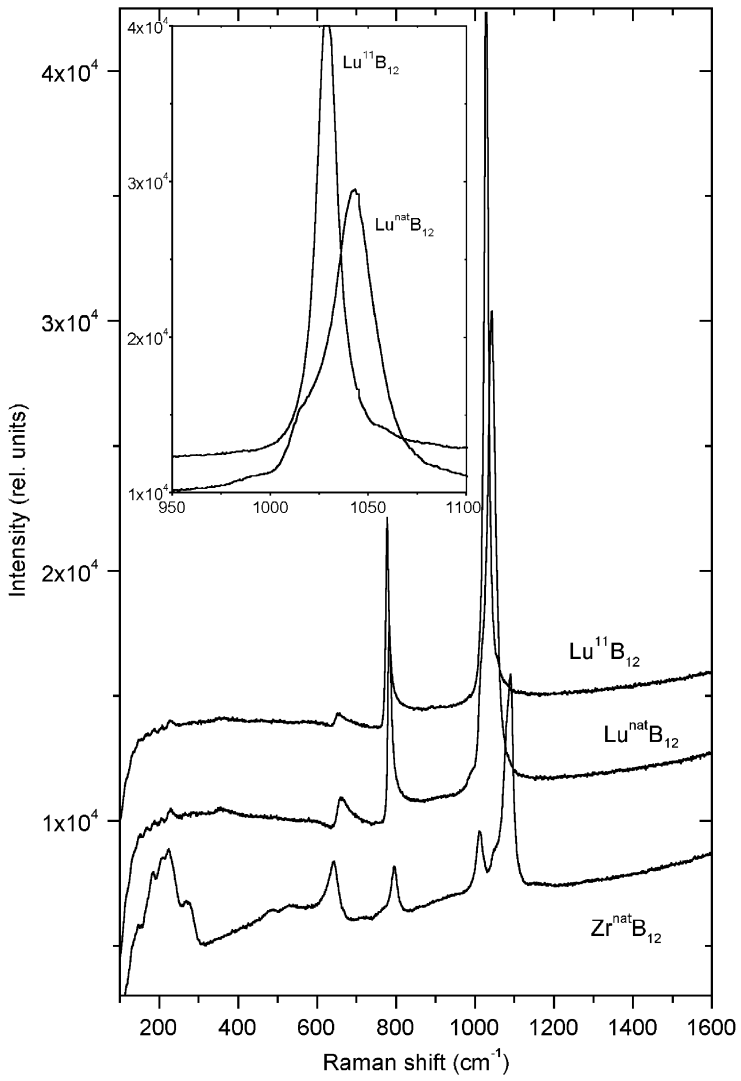

Fig. 1. Raman spectra of $Lu^{nat}B_{12}$, $Lu^{11}B_{12}$ and $Zr^{nat}B_{12}$. The insert shows the modification of the strongest Raman line of LuB_{12} by the influence of different isotope concentration.

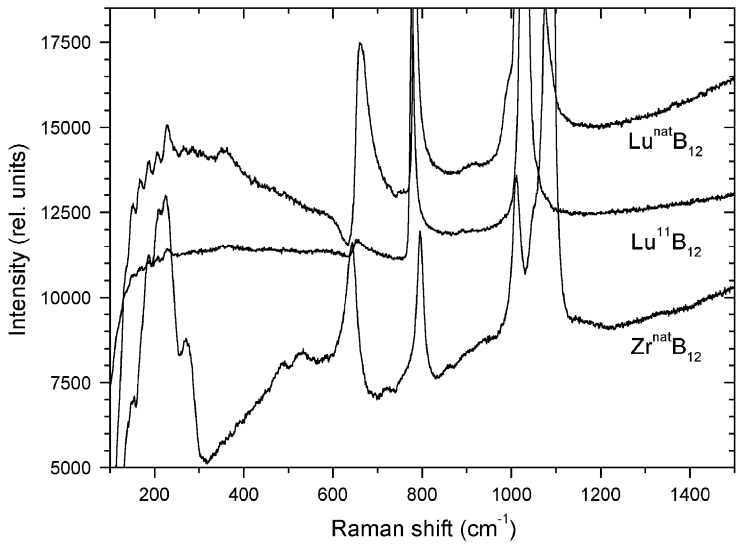

Fig. 2. Raman spectra of $Lu^{nat}B_{12}$, $Lu^{11}B_{12}$ and $Zr^{nat}B_{12}$ with improved signal-to-noise ratio (five-fold integration time compared with Fig. 1). The spectra are vertically shifted relative to one another.

Table 1
Raman frequencies of $Lu^{nat}B_{12}$, $Lu^{11}B_{12}$ and $Zr^{nat}B_{12}$ compared with Raman results of Fujita et al. [25] obtained from polarization-dependent measurements and data obtained from phonon spectra of Bouvet et al. [26] obtained by inelastic neutron scattering

LuB_{12}						ZrB_{12}	
$Lu^{nat}B_{12}$	$Lu^{11}B_{12}$ (this paper)		Fujita et al. [25]	Neutron scattering (Bouvet et al. [26])		$Zr^{nat}B_{12}$ (this paper)	
				~129	RE optical Mode		
152 (1)	152 (1)					151 (1)	
169 (1)	169 (1)					171 (1)	
187 (2)	187 (2)			~185	Opt. and rot. modes	187 (1)	
207 (1)	207 (1)					209 (2)	
228 (1)	228 (1)					224 (1)	
238 (2)	—	Weak shoulder					
247 (2)	—	Weak shoulder					
266 (2)	—			~265	Intermolecular	270 (1)	
285 (2)	—			~281	vibrations of the B_{12}		
300 (2)	—			……	cubo-octahedra		
310 (2)	—			Until			
328 (3)	—			……			
356 (3)	358 (3)			~386			
—	—		F_{2g} (~460 cm^{-1})			487 (2)	
						530 (2)	
581 (10)						583 (2)	
663 (2)	653 (2)	Strong, possibly degenerated	E_g (~650 cm^{-1})			642 (1)	Middle
						720 (2)	Weak
784 (1)	777 (1)	Strong, possibly degenerated	F_{2g} (~815 cm^{-1})			796 (1)	Middle
908 (5)	—	Weak				859 (2)	Weak
						893 (2)	Weak
						942 (2)	Weak
990 (3)	890 (3)	Weak shoulder					
1015 (2)	—	Shoulder	E_g (~1000 cm^{-1})			1012 (1)	middle
1043 (1)	1028 (1)	Strong	A_{1g} (~1070 cm^{-1})			1050 (2)	Weak
						1080 (2)	Shoulder
						1090 (1)	Strong
—	1058 (1)	Weak shoulder					
1155 (3)	1146 (2)	Very weak				1152 (5)	Weak
						1297 (4)	Very weak
1366 (2)	—	Very weak				1337 (4)	Weak

Arrows indicate obvious correlations between specific phonons of both compounds.

Table 2
Spectral position of the strongest Raman lines and the relation of the frequencies

$Lu^{nat}B_{12}$ (cm^{-1})	$Lu^{11}B_{12}$ (cm^{-1})	ω_1/ω_2
663	653	1.015 (4)
784	774	1.009 (2)
1043	1028	1.015 (1)

Taking into account a displacement of metal atoms in the crystal structure of ZrB_{12} [29] we performed a factor group analysis with zirconium atoms located on, e.g., Wyckoff position 24*e* revealing three additional modes ($A_{1g}+E_g+T_{2g}$) becoming Raman active. Considering the metal disorder and the low frequency of the observed broad structure in the Raman spectra, we suggest attributing the low-frequency intensity to vibrations of the displaced metal atoms.

5. Conclusion

Despite the good quality of the investigated ZrB_{12} and LuB_{12} single crystals, both compounds contain considerable amount of structural imperfections lifting the phonon selection rules. This leads to numerous detectable Raman peaks in spectral ranges, where only Raman-inactive vibrations are expected. In this context, we like to remark that the presence of structural defects (B vacancies) is compatible with the density measurements (see above).

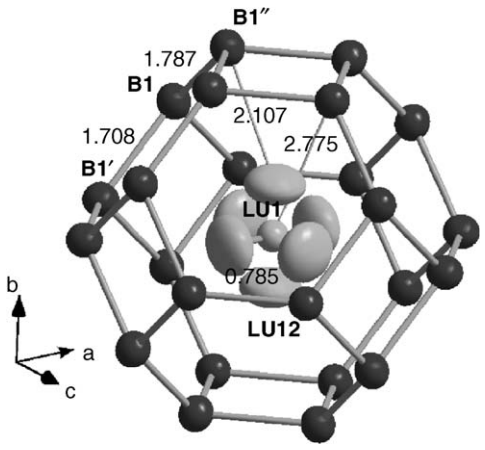

Fig. 3. Disorder of the metal atoms in LuB_{12}. B_{24} truncated octahedron with probability distribution of the displaced Lu atom (LU12) from the idealized center position (LU1). Displacement at 295 K and 0.361 Å. In ZrB_{12} the displacement is 0.388 Å [28].

Another independent confirmation of structural disorder in LuB_{12} and ZrB_{12} results from the structure refinements by X-ray investigations. While in the idealized structures the metal atoms are assumed to be accommodated exactly in the center of the cubo-octahedra, they are partly shifted towards the square segments of the truncated octahedra by 0.360 Å (4.84% of the lattice parameter a in LuB_{12}) and 0.388 Å (5.24% of a in ZrB_{12}), respectively, in the real structures (for ZrB_{12}, see also Fig. 3). This result immediately explains the occurrence of rather strong Raman lines in the low-frequency spectral range, where the lattice vibrations related to the movement of the metal atoms are expected. The sensitivity of Raman spectroscopy is underlined by the observation that the occupation densities of the disordered metal sites are only 1.33% for LuB_{12} [29] (for ZrB_{12} the according data are not yet available).

Moreover, point defects are certainly a likely reason for lifting the selection rules of Raman-inactive lattice vibrations. Although the influence of these intrinsic defects on the Raman spectra cannot be quantitatively given at present, Raman spectroscopy is obviously a sensitive tool to detect such structural distortions in boron-rich solids. In how far it is possible to correlate such Raman peaks to specific distortions or disorder phenomena will be subject of future investigations. Because of the strong influence of intrinsic structural imperfections on the electronic properties, as evidenced for β-rhombohedral boron and boron carbide, more detailed investigations of the real structure of these solids are highly desirable in order to gain a deeper understanding of the electronic structure of these compounds with complex building units in their crystal structures.

In parallel it will be studied, if the Jahn–Teller effect, which is responsible for distortions of boron cages in icosahedral boron-rich solids [3,4], is also a reason for structural distortion in the dodecaborides. A first experimental evidence for an elastic instability is the observation of a tetragonal distortion in LuB_{12} at low temperatures [30].

Comparing the Raman spectra of $Lu^{nat}B_{12}$ and $Lu^{11}B_{12}$ (see Figs. 1, 2 and Table 1) it is obvious that even the different boron isotopes, distributed in the B_{12} cubo-octahedra, are sufficiently strong imperfections to lift the selection rules. The distinct broad Raman signal at wave numbers below about 600 cm^{-1} occurs for $Lu^{nat}B_{12}$ only and is missing for $Lu^{11}B_{12}$. Moreover, several of the weak narrow Raman peaks visible in the case of natural isotope distribution are much weaker or even missing in the spectrum of isotope-enriched material. According to the neutron scattering experiments of Bouvet et al. [26] (see Table 1), most of these Raman peaks can be attributed to intermolecular vibrations of the cubo-octahedra, which would be Raman-inactive in a perfect structure.

References

[1] T. Serebriakova, V. Neronov, P. Peshev, Refractory borides, Metalurgia, M. (1991) (in Russian).
[2] V.I. Matkovich (Ed.), Boron and Refractory Borides, Springer, Berlin, Heidelberg, New York, 1977.
[3] R. Schmechel, H. Werheit, J. Phys.: Condens. Matter. 11 (1999) 6803.
[4] R. Schmechel, H. Werheit, J. Solid State Chem. 154 (2000) 61.
[5] D. Mandrus, B.C. Sales, R. Jin, Phys. Rev. B 64 (2001) 12302.
[6] J. Nagamatsu, N. Nakagawa, T. Muranaka, Nature 410 (2001) 63.
[7] V.V. Odintsov, Yu.B. Paderno, Yu.M. Goriachev, in: N.N. Sirota (Ed.), Chemical bond in semiconductor and semimetal crystals, Nauka I Tekhnika, Minsk, 1973, pp. 177–183 (in Russian).
[8] E.S. Konovalova, Yu.B. Paderno, in: V. Bamburov (Ed.), Vanadium and Boron compounds of rare earth elements, Ural Sci. Center, Sverdlovsk, 1982, pp. 28–52.
[9] H. Werheit, Boron compounds, in: O. Madelung (Ed.), Landolt-Boernstein, Numerical Data and Functional Relationshipsin Science and Technology, New Series, Group III, vol. 41D, Springer, Berlin, 1984, pp. 1–62.
[10] H. Werheit, Boron compounds, in: O. Madelung (Ed.), Landolt-Boernstein, Numerical Data and Functional Relationships in Science and Technology, New Series, Group III, vol. 17g, Springer, Berlin, 2000, pp. 1–491.
[11] B. Post, F. Glaser, J. Met. 4 (1952) 631.
[12] V. Matkovich, J. Economy, R. Giese, R. Barrett, Acta Crystallogr. 19 (1965) 1056.
[13] Yu. Paderno, B. Odintsov, I. Timofeeva, L. Klochkov, Teplofizika vysokich temperatur 9 (1971) 200 (in Russian).
[14] M. Arbusov, A. Adamovsky, A. Liashchenko, Powder Metall. 1 (1979) 50 (in Russian).
[15] K. Portnoi, V. Romashov, L. Burobina, Powder Metall. 7 (1970) 68 (in Russian).
[16] Yu.B. Paderno, A.B. Liashchenko, V.B. Filippov, A.V. Duchnenko, Science for Materials in the Frontier of Centuries: Advantages and the Challenges, in: V.V. Skorokhod (Ed.), IPMS NASU, Kiev, 2002, p. 34.
[17] I.R. Shein, A.L. Ivanovski, Phys. Solid State 45 (8) (2003) 1429–1434.
[18] B.T. Mattias, T.H. Geballe, K. Andres, E. Corenzwit, G.W. Hull, J.P. Majta, Science 159 (1968) 530.
[19] F. Glaser, B. Post, Trans. AIME 197 (1953) 1117.
[20] H. Okamoto, J. Phase Equilibr. 14 (2) (1993) 261.
[21] T. Massalski (Ed.), Binary alloy phase diagrams, ASMI, USA, 1996, p. 560.
[22] A. Leithe-Jasper, A. Sato, T. Tanaka, Z. Kristallogr. NCS 217 (2002) 9.

[23] Y. Paderno, V. Filippov, N. Shitsevalova, Jap. J. Appl. Phys. Ser. 10 (1994) 154–155.
[24] N. Shitsevalova, Thesis, 2001.
[25] Y. Fujita, N. Ogita, N. Shimizu, F. Iga, T. Takabatake, M. Udagawa, J. Phys. Soc. Jpn. 68 (1999) 4051–4052.
[26] A. Bouvet, T. Kasuya, M. Bonnet, L.P. Regnault, J. Rossat-Mignod, F. Iga, B. Fåk, A. Severing, J. Phys.: Condens. Matter. 10 (1998) 5667–5677.
[27] E.V. Nefeodova, P. Alekseev, J.-M. Mignot, V.N. Lazukov, I.P. Sadikov, Yu.B. Paderno, N.Yu. Shitsevalova, R.S. Eccleston, Phys. Rev. B 60 (1999) 13507–13514.
[28] K.S. Nemkovski, P.A. Alekseev, J.-M. Mignot, N.N. Tiden, Phys. Stat. Sol. (c) 1 (11) (2004) 3093–3096.
[29] A. Pietraszko, INTAS Meeting, Kosice, Slovakia, December 17, 2004.
[30] A. Pietraszko, private communication, 2005.